# On-chip mid-infrared optical sensing with GeSbSe waveguides and resonators

MICHAEL GRAYSON,[1] GREG KRUEPER,[2] BO XU,[2] MO ZOHRABI,[1] DAG HJELME,[3] JULIET T. GOPINATH,[1,2,4] AND WOUNJHANG PARK[1,4,*]

[1]*Department of Electrical, Computer and Energy Engineering, University of Colorado, Boulder, CO 80309, USA*
[2]*Department of Physics, University of Colorado, Boulder, CO 80309, USA*
[3]*Department of Electronic Systems, Norwegian University of Science and Technology, Trondheim, Norway*
[4] *Materials Science and Engineering Program, University of Colorado, Boulder, CO 80309, USA*
*won.park@colorado.edu*

**Abstract:** We fabricated single mode $Ge_{28}Sb_{12}Se_{60}$ waveguides and resonators using e-beam lithography and achieved a propagation loss of 3.88 dB/cm at 3.66 μm. We compared $BCl_3$ and $CHF_3$ etch chemistries and determined $CHF_3$ produced 1.5 dB/cm higher propagation losses at 3.6 μm due to C-H bond absorption. We use fabricated waveguides to detect an aromatic aldehyde dissolved in a non-polar solvent with a limit of detection of 1.09 μmol/mL. We then reduce this detection limit to 0.25 μmol/mL using the enhancement produced by a chalcogenide ring resonator.

## 1.    Introduction

Chalcogenides are a promising material for linear and nonlinear optics in the mid infrared (MIR) [1]. They have high nonlinearity, low material absorption loss, and are easily deposited using a wide variety of techniques [2–4]. In particular, $Ge_{28}Sb_{12}Se_{60}$ (GeSbSe) is transparent between 1 to 15 μm and has a high nonlinear figure of merit [1,2,5]. Impurity absorption will limit the transmissions of fabricated waveguides. These occur at 2.9 μm for OH bonds, 3.4 μm for CH bonds and 4.6 μm for SeH bonds [3,6]. GeSbSe has been shown to be non-cytotoxic, making it particularly useful for bio-sensing in the MIR [7,8]. Previous demonstrations of chalcogenide photonic devices in the MIR have shown resonator quality factors up to $2 \times 10^5$ in $As_2Se_3$ at 5.2 μm [9] and propagation losses as low as 0.3 dB/cm at 3.5 μm in GeAsSe [10]. These demonstrations were in large waveguides, supporting multiple modes. The large waveguide dimensions reduce the contribution of surface absorption to the total propagation loss. However, for some applications such as high evanescent field sensors or dispersion engineered devices, single mode waveguides are required [11,12]. By single mode we mean an optical waveguide with one transverse electric (TE) and one transverse magnetic (TM) mode. Single mode operation will increase the field overlap with absorbing contaminants produced on the surface of the waveguide during fabrication. This means that the surface contamination must be much better controlled in a single mode device than in multimode waveguides. In this paper, we demonstrate single-mode waveguides and micro-resonators for spectroscopy at 3-4 μm.

    One of the primary applications for MIR photonic devices is sensing organic compounds [8,13]. The MIR region is known as the molecular fingerprint region, where organic molecules have unique absorption spectra [8,14]. The wavelength region of 3-4 μm primarily contains the vibrational resonances of C-H bonds [15]. These peaks are very strong and consist of many sub-peaks, each of which corresponds to a different combination of the collective stretching of the C-H bonds in the molecule [16]. The measurement of the C-H bonding peaks alone cannot be used to completely differentiate between chemicals unless performed at a low temperature

[17] due to the large linewidth. However certain functional groups such as benzene rings, or aldehydes can result in a measurable splitting of C-H vibrational resonances [17]. We therefore choose to focus on a particular class of chemicals, the aldehydes, which have absorption bands in the 3.5-3.8 µm region where our waveguides and resonators function with the lowest loss [18]. These peaks correspond to the C-H stretching of the aldehyde group and have fine structure in this region that would allow our waveguides to differentiate between different aldehydes [19–21]. Aldehydes such as acetaldehyde are a prime candidate for sensing as they are extremely common as a pollutant or metabolite [22–25] as well as a useful manufacturing product [26] but are a potent carcinogen [24]. In this study, we choose to detect trans-cinnamaldehyde as it demonstrates sensing of the characteristic aldehyde peak at 2730 cm$^{-1}$ [21], and is a nontoxic, useful industrial compound [26–29]. In this study, we sense aldehydes using the evanescent field of waveguides. Evanescent waveguide sensing provides the benefit of physical size reduction without loss of sensitivity and robustness [13].

Previously demonstrated chalcogenide waveguides operating at 3-4 µm used a CHF$_3$ etch chemistry to produce losses as low as 0.3 dB/cm [10,30]. However, CHF$_3$ etch passivates with a flouropolymer that also contains C-H bonds, which have significant absorption at 3.4 µm [31]. To reduce the loss contribution of the background absorption by the fluoropolymer and other contaminants, the waveguides were made to be very large (8 µm$^2$). This reduces the amount of evanescent field which interacts with the surface contaminants. There are other previous demonstrations at 1.5 µm that used chlorine etch chemistry. This etch chemistry produces lower losses at 1.5 µm than CHF$_3$ etches [32]. Chlorine chemistry will minimize impurities with C-H bonding as it passivates through a B$_2$Cl$_4$ polymer with no C-H bonding [33–35]. The B-Cl bond consists of heavy atoms and simulations of the vibration spectra show it does not have resonances in the 3-4 µm [36].

In this work, we present the design and fabrication of low loss single mode GeSbSe waveguides and resonators and demonstrate chemical sensing in the MIR. The fabrication employed e-beam lithography and two different reactive ion etching methods to show that BCl$_3$ etch chemistry performed better than commonly used CHF$_3$ etch chemistry. Finally, we demonstrate the sensing of an aromatic aldehyde using a waveguide and a resonator with high accuracy.

## 2.    Fabrication of waveguides and resonators

Waveguides and resonators were fabricated through a combination of thermal evaporation, electron beam lithography (EBL), and inductively coupled plasma (ICP) reactive ion etching (RIE). MgF$_2$ substrates with <100> surface orientation, 0.5 mm thickness, and 0.5 nm surface roughness were obtained from Biotain Crystal. The substrates were oriented with <101> planes on either edge intended for cleaving to ensure right angled cleaves. GeSbSe films were thermally evaporated at 10$^{-7}$ torr with an initial deposition rate of 1 Å/s which was increased to 10 Å/s after 100 nm. If the film was deposited at 10 Å/s from the beginning, we observed a large amount of bubbles in the film after annealing due to the diffusion and accumulation of trapped gas. Next, the films were annealed at 265 °C under a nitrogen atmosphere to promote adhesion between the chalcogenide and the MgF$_2$ while reducing thermal stress. Without this process the chalcogenide films would delaminate during the EBL process. EBL was performed at the Nanofabrication Facility at the University of California Santa Barbara. We used a positive CSAR resist with a thickness of 530 nm, and a 10 nm thick Au charge compensation layer. The exposure conditions were as follows: 100 kV with 2 nA current and a dose of 350 µC/cm$^2$.

Two different etch chemistries, BCl$_3$/Cl$_2$ and CHF$_3$, were used for RIE as the final step of the fabrication. All etches were performed on a Si carrier wafer with a 500 nm thick thermal SiO$_2$. Before each etch, the chamber was cleaned with an O$_2$ plasma and conditioned by running the etch with no sample. The etch was very sensitive to the condition of the chamber and the etch rate is usually very high until multiple etches were run. Samples fabricated with standard

photolithography were used to calibrate the etch rate before the EBL samples were etched. Usually 4-5 etches were required before the etch rate reached a steady value.

The $CHF_3$ etch chemistry was optimized based on the results from Choi *et al.* [31]. We observed similar trends in ICP power, RF power and gas flow rate. However, in our optimization we observed a much larger amount of grass growth. We found that increasing the ICP power, reducing the pressure and adding oxygen removed the grass. The final etch used 2 sccm of $O_2$, 25 sccm $CHF_3$, 600 W ICP power, 60 W bias power, and 3 mTorr pressure. The etch rate of GeSbSe was on average 23 nm/s. For the $BCl_3/Cl_2$ etch, the conditions were 5 sccm of $Cl_2$, 10 sccm of $BCl_3$, 500 W ICP, 100 W bias power and 3 mTorr. The resulting etch rate was 36.4 nm/s. The selectivity between GeSbSe and resist is the same for both etches at 3:1. Figure 1(a), (c) show scanning electron microscopy (SEM) images of the $BCl_3/Cl_2$ etched waveguides while Fig. 1(b), (d) show the $CHF_3$ etches at different stages of fabrication.
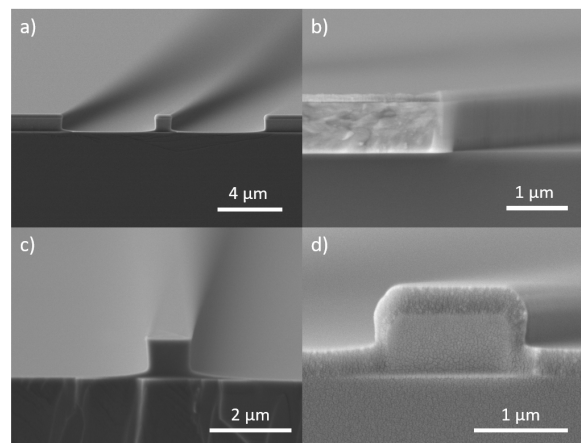


**Fig. 1.** (a) An image of a GeSbSe waveguide after $BCl_3/Cl_2$ etching. The resist can be seen as a thin layer on top of the chalcogenide. The substrate is $MgF_2$. (b) An image of an etched side wall of GeSbSe after $CHF_3$ etching and $O_2$ plasma ashing of the hardened resist. (c) An image of the fabricated waveguide using a $BCl_3$ etch chemistry after resist removal. (d) An image of a waveguide fabricated with $CHF_3$ etch chemistry then cleaned and cladded with 350 nm of $CHF_3$ flouropolymer.

After the ICP RIE process, the resist becomes hardened and difficult to remove. The top layer of the resist becomes insoluble in dimethyl sulfoxide (DMSO) and must be first removed with a chemical or physical plasma etch. Figure 1(a) shows an image of the waveguide with the plasma hardened resist on top. We used $O_2$ plasma with 100 W of power, 2 sccm $O_2$ at 350 mTorr for 35 seconds. The sample after this etch is shown in Fig. 1(b). The rest of the resist was removed by soaking the sample in a 80 °C DMSO bath for 2 minutes. We found that GeSbSe was etched in DMSO at a rate of 2 nm/min and could cause delamination if adhesion was poor. Figure 1(c) shows an image of a $BCl_3$ etched waveguide after the resist removal process. After this point, the sample was either measured within 30 minutes or a cladding was added immediately in order to minimize surface contamination.

For the cladding layer, we used Cytop 809M which is a flouropolymer with silane terminations for adhesion. Cytop was spin coated at 500 rpm to yield a 3 μm thick film. This sample was then annealed to cure the Cytop for 1 hr at 50 °C, 2 hrs at 80 °C and 2 hours at 200 °C. For sensing experiments, most of the Cytop was stripped by soaking the sample in the Cytop commercial solvent for 24 hours then sonicating. This left a 50 nm film of Cytop which was silane bound to the surface of the chip. These devices have a evanescent field factor of 0.43

which was sufficiently strong evanescent field for sensing. Additionally, we also investigated a plasma deposited flouropolymer cladding as described in [10]. This cladding was produced using conditions similar to our ICP RIE $CHF_3$ etch, but with negligible bias voltage and higher $CHF_3$ flow rate. The ICP RIE conditions were 50 sccm $CHF_3$, 1 W bias power, 300 W ICP power at 10 mTorr of pressure. The deposition rate was 50 nm/min. An image of the waveguide after plasma flouropolymer deposition is shown in Fig. 1(d). Before the flouropolymer or Cytop cladding was deposited, an $O_2$ plasma etch was performed to clean the sample. The cladding was then immediately deposited without breaking vacuum to prevent any exposure to ambient organic compounds, atmospheric reactions with the chalcogenide, or adsorption of water. Once the entire chip was fabricated, samples were cleaved using a scribe and applying gentle pressure to produce a smooth facet to couple light into.

## 3. Optical measurements of ring resonators

To characterize the loss in our waveguides, we measured the transmission of ring resonators with the same cross-sectional dimensions. Measurements were performed using an Argos Aculight Model 2400 CW optical parameteric oscillator (OPO), Bristol 671 wavemeter, and two PbSe AC coupled amplified detectors. The scanning of the laser and intensity detection was automated following the procedure described by Morrison *et al.* [37]. The OPO is continuously tunable over a 100 GHz range (4.3 nm) using piezo modulation of the 1064 nm seed laser and discretely tunable between 3.1 to 3.9 μm. A servo motor was additionally used for coarse wavelength tuning of the OPO. The laser produces 300 mW of continuous power at 3.5 μm. The power and polarization were controlled using a half wave-plate and polarizer. Neutral density filters were used to reach sub milliwatt powers for resonance measurements. The wavelength of the OPO was measured using the wavemeter which has 0.5 pm resolution at 3 μm. Two detectors, one for the input power and one for the output power are required for measuring the transmission of the chip. The output of the OPO was chopped at 200 Hz with a 50% duty cycle for AC coupled detection. A NI 6363 digital acquisition device was used to set the piezo voltages for fine wavelength tuning and record the voltages of the detectors. The wavemeter and the OPO controller were also remotely controlled. This was all integrated into a python software package that allowed for automated scanning at picometer resolution from 3.1 to 3.9 μm.

To couple to the waveguides, 0.56 numerical aperture (NA) molded asphere lenses with 4 mm focal length and 5 mm aperture were used. Stages were controlled with 3 axis differential micrometers and a single axis piezo. Light scattered from the chip was observed using a 25 mm focal length $CaF_2$ lens and a FLIR A6700SC InSb infrared camera. The resonances were measured over a large bandwidth with 13.8 pm increments. The results of these measurements for the Cytop cladded ring resonators fabricated using the $BCl_3/Cl_2$ and $CHF_3$ chemistries are shown in Fig. 2(a) and (b), respectively.

The resonators were both 1.3 μm wide, 0.88 μm tall, 150 μm in radius and point-coupled to a bus waveguide with a coupling gap of 1.05 μm. These resonators were chosen as they had both the highest Q factor and were the closest to critically coupled. Measurements were taken with TE polarization which had a lower loss than the TM mode. Higher losses observed with TM mode are due to the incomplete removal of e-beam resist during the fabrication process [10,30]. The wavelength scans were used to calculate the Q factor and free spectral range (FSR) of the resonators. Each resonance in Fig. 2(a) and (b) was fit with a Lorentzian function and the full width at half maximum was used to calculate the loaded Q-factor by $Q_l = \omega/\delta\omega$. The variations in the transmission of the waveguide is primarily due to changes in free space to chip coupling during the scan. At 3.53 μm, the loss of the waveguides increased significantly which prevented measurements of Q factor at shorter wavelengths for both samples. The loaded Q factors and coupling depths are shown in Fig. 2(c). The coupling depth here is $1 - T$, where T is the transmission. The resonators are mostly undercoupled with some of the $BCl_3/Cl_2$ etched
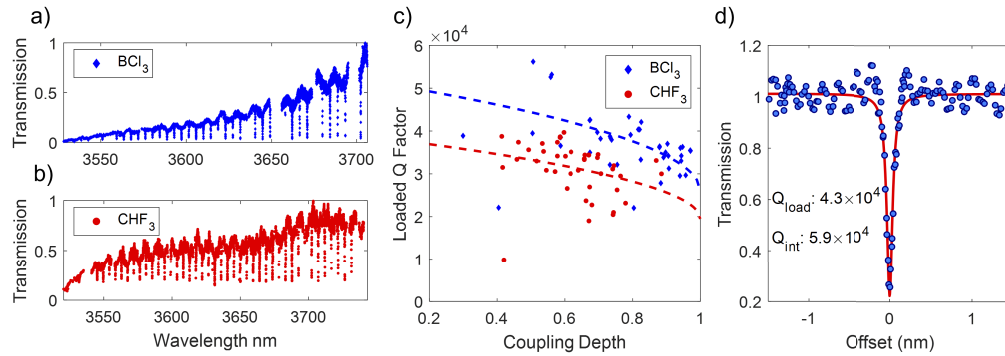
**Fig. 2.** (a) The transmission of a $BCl_3/Cl_2$ etched bus waveguide coupled to a 150 μm radius ring resonator with a height of 0.88 μm and a width of 1.3 μm. The gaps in the spectrum are due to loss of OPO resonance during the scan. The coupling is slowly lost as the laser scans down in wavelength. (b) The transmission of a $CHF_3$ etched bus waveguide coupled to a 150 μm radius ring resonator. The coupling is much more stable in this measurement and the OPO was operated at higher power resulting in better continuity of the scan. (c) The loaded Q factors and coupling depths of a single $CHF_3$ etched resonator and a single $BCl_3$ etched resonator taken from the scans in (a) and (b). The $BCl_3/Cl_2$ etched waveguide is in blue, while the $CHF_3$ etched waveguide is in red. The measured loaded Q factors are plotted as a function of coupling to determine the average intrinsic Q factor from 3.55 μm to 3.7 μm for each resonator. The coupling gaps between the waveguide and resonator are the same for both etch chemistries, but the $CHF_3$ etched resonators have lower Q factor resulting in undercoupling. The dashed lines represent a fit of Eq. [1] with the average intrinsic Q factors for each chip. (d) A plot of the highest measured intrinsic Q factor across both chips. This resonance occurred in the $BCl_3/Cl_2$ etched device at 3.61 μm. While higher Q factors were observed, the uncertainty in Q factor for these measurements was too high to guarantee they were higher than the average Q factor of $5.4 \times 10^4$ with 95% confidence.

resonators critically coupled. This can be seen with the loaded Q factor increasing with lower coupling depths. The intrinsic Q factors were then calculated using Eq. (1), Where $T$ is the on resonance transmission, $Q_l$ is the loaded Q, and $Q_i$ is the intrinsic Q factor [38].

$$Q_i = 2Q_l/(1 + \sqrt{T}).$$

(1)

For the high Q resonators considered here we approximate the on-resonance transmission T as the on-resonance to off-resonance power ratio. The highest statistically significant intrinsic Q factor was measured in the $BCl_3/Cl_2$ etched resonator, which is shown in Fig. 2(d). By statistically significant, we mean the uncertainty in Q factor for these measurements was low enough to guarantee they were higher than the average Q factor of $5.4 \times 10^4$ with 95% confidence. The intrinsic Q factor was $5.9 \pm 0.2 \times 10^4$. The effective group index can be calculated from the FSR of 4.23 nm to be 3.01.

Using the equation $\alpha = 2\pi n_g/(Q_i\lambda)$, where $ng$ is the group index, we calculated the propagation loss to be 3.88 dB/cm. This high loss factor is primarily due to absorption as the roughness of the waveguides was very low with a line roughness of 2 nm. Using the measured roughness and scattering theory [39], the scattering loss was estimated to be on the order of 0.1 dB/cm which is far lower than the values we have measured. The origin of these additional losses are likely due to some kind of atmospheric degradation that occurs in the chalcogenide films during the fabrication process as observed in other studies [10,40]. Our waveguides will suffer more from the surface-related losses because they are single mode waveguides with small cross-section while those demonstrated by Ma *et al.* [10] involved devices with much larger cross-sections.

Figure 3(a) shows a histogram of all the intrinsic Q factors measured from both the $BCl_3$ and $CHF_3$ resonators with the $BCl_3$ performing 33% better with statistical significance. This corresponds to a 1.5 dB/cm reduction in loss at 3.6 μm. Figure 3(b) shows a low resolution scan of the transmission of the $BCl_3$ and $CHF_3$ waveguides. The loss increases significantly in the $CHF_3$ etched waveguides when compared to the $BCl_3/Cl_2$ etched waveguides between 3.40 and 3.45 μm which matches the spectrum of losses in $CHF_3$ etched waveguides reported in literature [10,30]. This reduction of loss achieved by the chlorine-based RIE will be significant for low loss waveguides in the MIR. Additionally, $B_2Cl_4$ plasma deposited polymers could be used as a lower loss passivation layer than $CHF_3$ provided these polymers are stable in atmosphere.
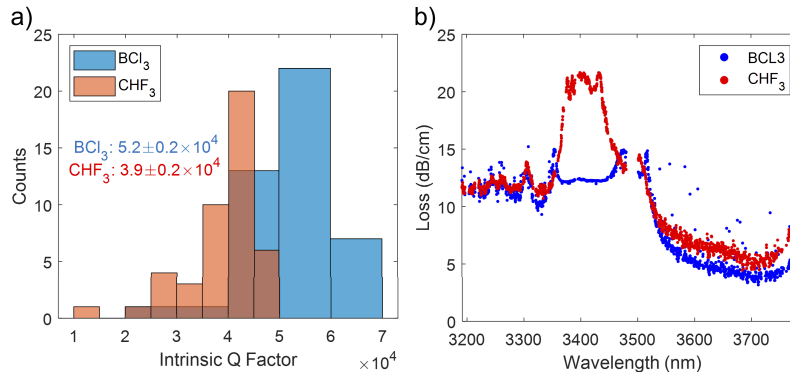


**Fig. 3.** (a) A histogram of all the intrinsic Q factors measured from both chips in two different resonators assuming undercoupling. Each resonator was identical with a radius of 150 μm, a height of 0.88μm, and a width of 1.3 μm. The uncertainty of the mean Q factor is the same in either measurement. The average loss of the $CHF_3$ etched resonators was 5.85 dB/cm while the average loss of the $BCl_3/Cl_2$ etched resonators was 4.38 dB/cm. (b) A plot of the loss of the waveguides over the entire bandwidth of the laser. The loss increases significantly below 3.5 μm This is likely due C-H bonding from hydrocarbons absorbed from atmosphere or from water in the sample. The peaks in the $CHF_3$ etched devices which are not in the $BCl_3/Cl_2$ etched devices are due to C-H bonding in the passivation layer. The increase in loss at 3.8 μm is due to C-F bonding.

The Q factors we observed in these devices are lower than what was previously reported [10]. For example, a loss of 0.3 dB/cm has been demonstrated in this wavelength region using GeAsSe waveguides [10]. GeAsSe is a very similar material to GeSbSe in terms of refractive index and absorption making a comparison of our waveguides to those produced by Ma *et al.* valid [41,42]. These waveguides were 7 times larger in cross-sectional area and thus had much weaker fields at the surface of the waveguide, which in turn resulted in lower absorption loss due to the surface adsorbed species. In contrast, our device is a single mode waveguide with a much stronger mode confinement factor and higher field at the waveguide surface. More specifically, our modes have 24% of the power outside of the waveguide in air, which is orders of magnitude larger than 0.32% in the prior work [10]. We can compare the actual field intensity at the surface of the waveguide through simulation. While the materials used for either case are different, the changes in material absorption will be negligible when compared to absorption due to contaminants from fabrication [41,42]. Changes in absorption due to refractive index changes are determined through optical mode simulations. Simulations were performed using COMSOL eigenmode solver. The cross sections for both the waveguides in our study and those in Ma *et al.* were simulated using the refractive indices from literature for the substrate, core, and cladding [10]. The increased sensitivity to surface contamination was determined by the ratio of the line integral of the normalized electric field intensity at the boundary of the waveguide for those

fabricated by Ma *et al* and our waveguides. The enhanced field at the surface in our waveguides will result in a 54 times higher absorption by the surface adsorbed species in our device than the previously demonstrated by Ma *et al*. [10]. This increases the sensitivity of the waveguide sensor, but it also makes the device more susceptible to contaminants from the atmosphere and fabrication processes. Assuming 0.1 dB/cm of material absorption and 0.1 dB/cm of scattering [10,39] we would expect a loss of 5.4 dB/cm in our waveguides if we had the same amount of surface absorption due to contamination as in the prior work [10]. This shows that, while the total loss in our device is higher than that of the previously demonstrated, it is mainly due to the smaller waveguide cross-section. The absorption per fraction of evanescent field is actually lower. Specifically, the absorption loss per fraction of evanescent field is 30% lower in the $BCl_3/Cl_2$ etched resonators as in the previously reported $CHF_3$ etched waveguides [10].

Ma *et al.* reported that $O_2$ plasma cleaning improved the loss of their waveguides. However we found that $O_2$ ashing increased our loss significantly. All waveguides fabricated were $O_2$ plasma ashed during fabrication. This unfortunately, will result in absorption losses. These losses are necessary as the EBL resist must be removed to allow the waveguides to be functional. We mitigated these losses by removing only a small portion of the resist with an $O_2$ ash. The rest of the resist was stripped with DMSO. The loss due to oxygen ashing could be recovered by etching the waveguides with an HF solution. This implies the oxygen plasma generated some kind of absorbing oxide. This oxide could also be removed by a hydrogen plasma which would prevent exposure of the sample to water, which occurs in the HF solution. Cytop cladding and annealing were the only processes that improved the Q factor. This is likely due to the cytop curing process which desiccates the sample. Lin *et al.* also reported a reduction in loss after annealing due to the evaporation of water and volatile organics [40]. We also found that using an argon clean in place of an $O_2$ ash and a flourinated polymer did not improve the sample either. This is likely due to the absorption by the flouropolymer layer whose effect is magnified because of our small device cross-section. We also observed degradation when exposed to atmosphere for 24 hours, which is consistent with previous studies [10,40]. Previous studies on the degradation of chalcogenide films show that carbon is adsorbed on the chalcogenide surface when exposed to atmosphere [43]. These carbon impurities could form a variety of bonds that will absorb in the 3-4 μm region. To reduce these losses further, it will be necessary to passivate the GeSbSe film immediately after evaporation, preferably in vacuum. This could be done with a thin layer of $MgF_2$, GeSbS, or Cytop. After etching, the sample will need to be passivated again. We additionally did not perform any cleaning of our $MgF_2$ substrates which may also introduce loss at the bottom surface of the waveguides.

## 4.  Optical sensing of aromatic aldehyde

The large amount of evanescent field that induces larger absorption loss in our waveguide makes them sensitive to the absorption of chemicals for spectroscopy. Performing absorption spectroscopy in waveguides can enhance the sensitivity through reduction in the group velocity or through resonantly enhancing the field strength in a resonator [44,45]. Spectroscopy in waveguides additionally has the benefit of stability, small footprint, and integration with other devices such as microfluidic channels, detectors, and laser sources [8,46–48].

Sensing experiments were performed using a 1.2 μm by 0.88 μm waveguide cladded with a 50 nm of Cytop to prevent adsorption of chemical compounds onto the chalcogenide surface. Waveguides with smaller width were used to maintain critical coupling with a thinner cladding. Changes in the transmission of the waveguide when exposed to an analyte were used to determine the concentration. Small concentrations of trans-cinnamaldehyde was dissolved in $C_2Cl_4$ which is a common solvent for Fourier transform infrared spectroscopy. Concentrations were prepared using a microliter pipette and an ultra micro-balance. These solutions were deposited on top of a waveguide and the change in transmission was measured. A basic overview of the sensing

experiment is shown in Fig. 4. The evanescent field of the waveguide shown in Fig. 4 is absorbed by the chemical dissolved in the solvent. This results in a change in transmission of the waveguide. Light was coupled into a 7.63 ± 0.04 mm long waveguide and 60 μL of solution was deposited on top of the waveguide. The total coupling efficiency was recorded and a scan of the transmission over wavelength was taken. After each measurement, the sample was cleaned with solvent and then re-coupled. The results of these measurements are shown in Fig. 5(a). The background fluctuations in the signal are due to Fabry-Perot resonances in the waveguide. The transmission of the waveguide is reduced as the concentration is increased, as expected. In these measurements, the wavelength range of the scan was reduced to minimize the evaporation of the solution during the measurement. The time required for each measurement was 5 minutes, while the time required for the solvent to totally evaporate was 1.5 hours. Assuming the evaporation is initially linear this will result in at most a 5% bias in the concentrations. Another source of uncertainty was the coupling efficiency through the chip which changed due to vibrations in the setup. This value could change by up to 5% through the entire scan. Figure 5(b) shows the absorbance of the waveguides for the different concentrations of cinnamaldehyde after removing the transmission of the pure $C_2Cl_4$ solvent. The Fabry-Perot fringes are partially removed by removing the background.
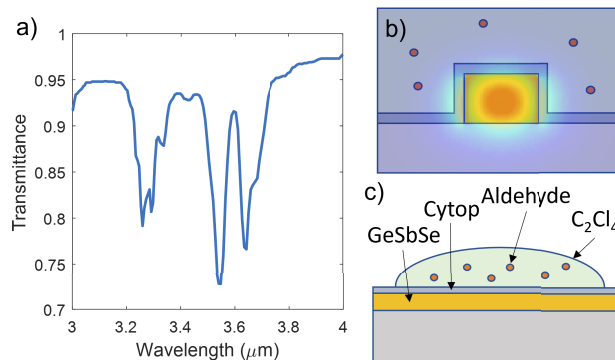


**Fig. 4.** a) Plot of the transmittance of cinnamaldehyde from 3 to 4 μm [21]. The resonances all correspond to C-H vibrational stretching, but the peaks at 3.54 μm and 3.66 μm are red shifted due to the aldehyde group. This red shifting of the C-H resonance allows us to operate in the region where our waveguides are most transparent. b) A depiction of the waveguide cross-section overlaid with a simulated TE mode. The evanescent field of the TE mode extends in the the solvent and is absorbed by the cinnamaldehyde. c) A depiction of the layers involved in the sensing experiment. The waveguides are fabricated with a thin (50 nm) layer of Cytop for protection. A 60 μL droplet of $C_2Cl_4$ with a known concentration of cinnamaldehyde is then deposited on the surface.

The change in the loss of the waveguide is calculated using Eq. (2), where $\alpha$ represents the raw change in loss of our sensor, $T$ is the transmission, $C_e$ is the coupling efficiency, and $L$ is the waveguide length.

$$T = C_e \exp(-\alpha L). \qquad (2)$$

To obtain the actual loss of the solution this loss must be divided by the confinement factor of the mode [11]. The confinement factor of our mode in $C_2Cl_4$ was calculated to be 0.426. The loss of each measurement as a function of concentration is shown in Fig. 6(a). The uncertainty of the loss includes the uncertainty in the length and the noise in the absorbance measurements. These points are fit to a linear regression whose slope is 0.63 ± 0.03 (dB mL)/(μmol cm) and an intercept of 0.3 ± 0.2 dB/cm. The limit of detection (LOD) of this device can be calculated using the $3\sigma$ criteria as $LOD = 3.3\sigma_y/m$, where $\sigma_y$ is the variance in the y-intercept and $m$ is the slope.

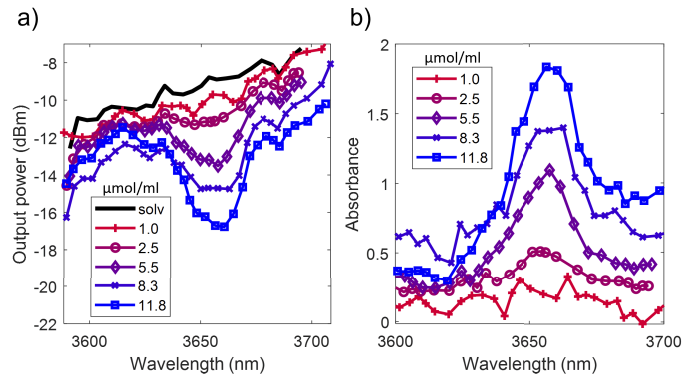a)                                                    b)



**Fig. 5.** (a) Raw output power of the waveguide with concentrations of cinnamaldehyde in $C_2Cl_4$ from from 1 to 12 µmol/mL. This value does not include loss due to coupling efficiency, which was measured independently for each concentration. The coupling efficiency was 16% on average. The input power used was on average 1.28 mW. The waveguide used for sensing was 0.88 µm in height and 1.2 µm in width. The background of the solvent is shown in black. Each concentration of cinnamaldehyde in $C_2Cl_4$ in µmol/ml is listed in the legend located in the lower left. The intensity signal alone has low noise compared to the changes due to absorption, but the Fabry-Perot oscillations are large. (b) Plot of the absorbance of each solution calculated by dividing the transmission of the waveguide with pure solvent. Large fluctuations are due to the Fabry-Perot oscillations. When calculating absorption, the raw signal was integrated from 3.64 to 3.68 µm.

The limit of detection for this measurement is 1.09 µmol/mL. To enhance the sensitivity, we performed similar measurements with a 50 µm radius ring resonator. The resonator will enhance the absorption of the analyte by the longer effective length of the cavity (3.04 mm) [44,49].

The resonator used for sensing experiments had a radius of 50 µm, a height of 0.88 µm and a width of 1.3 µm. The radius was reduced to increase the enhancement in sensitivity due to effective length while the width was increased to maintain critical coupling. The loaded Q factor did not change significantly from this reduction in radius. The average intrinsic Q-factor with solvent on the resonator was measured to be $1.57 \times 10^4$. The effective length is given by [Eq. (3)],

$$L_{eff} = \Gamma \frac{Q_i \lambda}{2\pi n_g}. \tag{3}$$

where $\Gamma$ is the confinement factor, $Q_i$ is the intrinsic Q factor, and $n_g$ is the effective group index. The effective length of these resonators is calculated to be 3.04 mm which gives an enhancement factor of 9.67.

These experiments were performed in a similar manner to the waveguide measurements except wavelength was scanned over a narrow range containing the resonance. The resonant wavelength we targeted was 3.664 µm which was close to the peak absorption of trans-cinnamaldehyde as shown in Fig. 4. The slope of this measurement was $5.5 \pm 0.3$ (dB mL)/(µmol cm) and the intercept was $0.2 \pm 0.4$ dB/cm. While the slope did increase by a factor of 8.7, the noise in the measurements also increased. The limit of detection of the resonator is 0.25 µmol/mL which corresponds to a realized detection enhancement by a factor of 4.4. The experimental enhancement does not match the theoretical value due to the uncertainty in the Q factor measurements. Figure 6(c) shows a plot of each loss measurement with the resonator enhancement and the confinement factor of the waveguide removed. These values will represent the actual molar attenuation of cinnamaldehyde at this wavelength. The slope of the linear fit corresponds to a molar attenuation of $354 \pm 9$ L $mol^{-1}$ $cm^{-1}$ at 3.66 µm. The LOD of 0.25 µmol/mL or 0.03 mg/mL is competitive with other
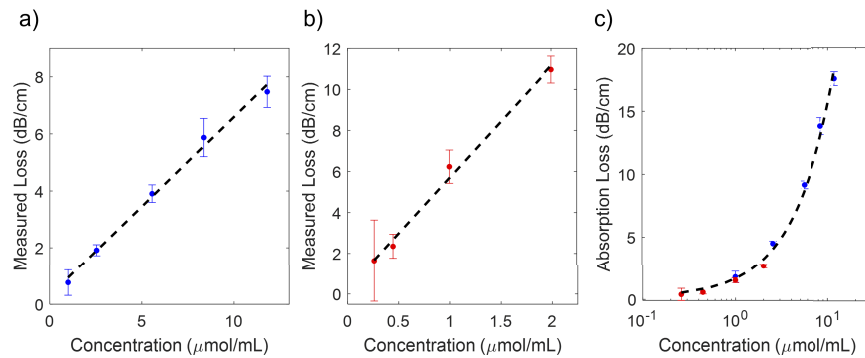
**Fig. 6.** a) Plot of the change in loss of the waveguide in dB/cm as a function of concentration of cinnamaldehyde in $C_2Cl_4$. The error bars are calculated using the standard deviation in the length of the waveguide and the variance of the intensity measurement for each scan. Linear regression was performed on these points to determine the LOD of 1.09 µmol/mL. b) A plot of the measured loss of a 50 µm resonators with different concentrations of solvent place on top. The loss was measured by measuring the intrinsic Q factor of the device using the same method as in Fig. 5(d). The loss of a resonator coated in pure solvent was then subtracted from these measurements to produce these values. This curve was also fit to a linear regression to obtain a LOD of 0.25 µmol/mL. The increased slope and lower LOD are due to the resonant enhancement of the cavity. For high Q factors or large concentrations this curve will not be linear as the enhancement and therefore slope will change with concentration. c) A plot of the true absorption of the cinnamaldehyde at various concentrations in $C_2Cl_4$. In these plots the evanescent field ratio for the waveguide and the enhancement from the resonator are remove using theoretical calculations. These points are then fit using linear regression to obtain a molar absorptivity of $354 \pm 9$ L mol$^{-1}$ cm$^{-1}$ at 3.66 µm.

demonstrations of optical sensing in the MIR [8]. This is to our knowledge the first demonstration of resonant absorption spectroscopy on chip at 3.6µm [8]. The low Q factor observed in the resonators is the primary limitation for acheiveing lower limits of detection. Having a higher Q factor would significantly increase the absorption enhancement and additionally would be less affected by the Fabry-Perot fringes in the waveguide transmission.

## 5.    Conclusion

In conclusion, we have designed and fabricated GeSbSe waveguides and ring resonators using EBL and ICP RIE etching for operation in the MIR. We calibrated both $CHF_3$ and $BCl_3/Cl_2$ etch chemistries for the fabrication of low loss GeSbSe waveguides. We observed that using $BCl_3/Cl_2$ etch resulted in a 1.5 dB/cm reduction in loss compared to $CHF_3$ etch, which is a significant difference for producing low loss waveguides in the MIR. While the losses we achieved were higher than previously demonstrated, this was only due to the small waveguide cross-section and the consequent increase in the mode fraction outside the waveguide which was required for single-mode operation. The absorption loss per fraction of evanescent field we demonstrate is twice as low as previous studies [10]. Using these fabricated waveguides we detected trans-cinnamaldehyde in $C_2Cl_4$ using a C-H vibrational peak which is unique to aldehydes. Using the waveguides, we achieve a LOD of 1.09 µmol/mL and obtain an even lower value of 0.25 µmol/mL using the resonant enhancement. We calculate the molar absorptivity of cinnamaldehyde to be $354 \pm 9$ L mol$^{-1}$ cm$^{-1}$ at 3.66 µm. The sensitivities of these devices could be significantly enhanced by reducing the contamination of the waveguides by species containing C-H bonding from the atmosphere and fabrication. The absorption of GeSbSe at this wavelength

is low enough to allow for Q factors up to $10^6$. This would enable the use of nonlinearity for spectroscopic measurements, allowing for a much wider variety of devices and applications. The high field intensities achieved in these resonators could also pave the way for the study of strong coupling between vibrational modes of molecules and an optical field.

**Disclosures.** The authors declare no conflicts of interest.

**Data availability.** Data may be obtained from authors upon reasonable request.

## References

1. B. J. Eggleton, B. Luther-Davies, and K. Richardson, "Chalcogenide photonics," Nat. Photonics **5**(3), 141–148 (2011).
2. L. Petit, N. Carlie, H. Chen, S. Gaylord, J. Massera, G. Boudebs, J. Hu, A. Agarwal, L. Kimerling, and K. Richardson, "Compositional dependence of the nonlinear refractive index of new germanium-based chalcogenide glasses," J. Solid State Chem. **182**(10), 2756–2761 (2009).
3. V. S. Shiryaev and M. F. Churbanov, "1 - Preparation of high-purity chalcogenide glasses," in *Chalcogenide Glasses*, J.-L. Adam and X. Zhang, eds. (Woodhead Publishing, 2014), pp. 3–35.
4. J. Orava, T. Kohoutek, and T. Wagner, "9 - Deposition techniques for chalcogenide thin films," in *Chalcogenide Glasses*, J.-L. Adam and X. Zhang, eds. (Woodhead Publishing, 2014), pp. 265–309.
5. Glass Schott, "Infrared Chalcogenide Glass IRG 25," (2019).
6. S. Danto, D. Thompson, P. Wachtel, J. D. Musgraves, K. Richardson, and B. Giroire, "A Comparative Study of Purification Routes for $As_2Se_3$ Chalcogenide Glass," Int. J. Appl. Glass Sci. **4**(1), 31–41 (2013).
7. D. Mabwa, T. Kubiena, H. Parnell, R. Su, D. Furniss, Z. Tang, R. Leach, T. M. Benson, C. A. Scotchford, and A. B. Seddon, "Evaluating the cytotoxicity of Ge–Sb–Se chalcogenide glass optical fibres on 3T3 mouse fibroblasts," RSC Adv. **11**(15), 8682–8693 (2021).
8. V. Mittal, G. Z. Mashanovich, and J. S. Wilkinson, "Perspective on Thin Film Waveguides for on-Chip Mid-Infrared Spectroscopy of Liquid Biochemical Analytes," Anal. Chem. **92**(16), 10891–10901 (2020).
9. H. Lin, L. Li, Y. Zou, S. Danto, J. D. Musgraves, K. Richardson, S. Kozacik, M. Murakowski, D. Prather, P. T. Lin, V. Singh, A. Agarwal, L. C. Kimerling, and J. Hu, "Demonstration of high-Q mid-infrared chalcogenide glass-on-silicon resonators," Opt. Lett. **38**(9), 1470–1472 (2013).
10. P. Ma, D.-Y. Choi, Y. Yu, X. Gai, Z. Yang, S. Debbarma, S. Madden, and B. Luther-Davies, "Low-loss chalcogenide waveguides for chemical sensing in the mid-infrared," Opt. Express **21**(24), 29927–29937 (2013).
11. M. Vlk, A. Datta, S. Alberti, H. D. Yallew, V. Mittal, G. S. Murugan, and J. Jágerská, "Extraordinary evanescent field confinement waveguide sensor for mid-infrared trace gas spectroscopy," Light: Sci. Appl. **10**(1), 26 (2021).
12. S. Fujii and T. Tanabe, "Dispersion engineering and measurement of whispering gallery mode microresonator for Kerr frequency comb generation," Nanophotonics **9**(5), 1087–1104 (2020).
13. T. Schädle and B. Mizaikoff, "Mid-Infrared Waveguides: A Perspective," Appl. Spectrosc. **70**(10), 1625–1638 (2016).
14. H. Lin, Z. Luo, T. Gu, L. C. Kimerling, K. Wada, A. Agarwal, and J. Hu, "Mid-infrared integrated photonics on silicon: a perspective," Nanophotonics **7**(2), 393–420 (2017).
15. P. J. Larkin, "Chapter 6 - IR and Raman Spectra–Structure Correlations: Characteristic Group Frequencies," in *Infrared and Raman Spectroscopy (Second Edition)*, P. J. Larkin, ed. (Elsevier, 2018), pp. 85–134.
16. P. J. Larkin, "Chapter 7 - General Outline for IR and Raman Spectral Interpretation," in *Infrared and Raman Spectroscopy (Second Edition)*, P. J. Larkin, ed. (Elsevier, 2018), pp. 135–151.
17. P. J. Larkin, "Chapter 5 - Origin of Group Frequencies," in *Infrared and Raman Spectroscopy (Second Edition)*, P. J. Larkin, ed. (Elsevier, 2018), pp. 75–84.
18. R. L. Hudson and R. F. Ferrante, "Quantifying acetaldehyde in astronomical ices and laboratory analogues: IR spectra, intensities, 13C shifts, and radiation chemistry," Mon. Not. R. Astron. Soc. **492**(1), 283–293 (2020).
19. NIST, "Ethyl Vanillin," NIST Chemistry WebBook (2018).
20. NIST, "Benzaldehyde," NIST Chemistry WebBook (2018).
21. NIST, "2-Propenal, 3-phenyl-," NIST Chemistry WebBook (2018).
22. K. Mitsubayashi, G. Nishio, M. Sawai, T. Saito, H. Kudo, H. Saito, K. Otsuka, T. Noguer, and J.-L. Marty, "A bio-sniffer stick with FALDH (formaldehyde dehydrogenase) for convenient analysis of gaseous formaldehyde," Sens. Actuators, B **130**(1), 32–37 (2008).

23. K. Iitani, P.-J. Chien, T. Suzuki, K. Toma, T. Arakawa, Y. Iwasaki, and K. Mitsubayashi, "Fiber-Optic Bio-sniffer (Biochemical Gas Sensor) Using Reverse Reaction of Alcohol Dehydrogenase for Exhaled Acetaldehyde," ACS Sens. **3**(2), 425–431 (2018).

24. T. Salthammer, S. Mentese, and R. Marutzky, "Formaldehyde in the Indoor Environment," Chem. Rev. **110**(4), 2536–2572 (2010).

25. V. L. Dellarco, "A mutagenicity assessment of acetaldehyde," Mutat. Res. Genet. Toxicol. **195**(1), 1–20 (1988).

26. T. Bayer, A. Becker, H. Terholsen, I. J. Kim, I. Menyes, S. Buchwald, K. Balke, S. Santala, S. C. Almo, and U. T. Bornscheuer, "LuxAB-Based Microbial Cell Factories for the Sensing, Manufacturing and Transformation of Industrial Aldehydes," Catalysts **11**(8), 953 (2021).

27. F. A. Al-Bayati and M. J. Mohammed, "Isolation, identification, and purification of cinnamaldehyde from Cinnamomum zeylanicum bark oil. An antibacterial study," Pharm. Biol. **47**(1), 61–66 (2009).

28. M. Katayama, Y. Mukai, and H. Taniguchi, "High-performance liquid chromatographic determination of cinnamaldehyde," Analyst **115**(1), 9–11 (1990).

29. C. Liao, J. Shi, M. Zhang, R. Dalapati, Q. Tian, S. Chen, C. Wang, and L. Zang, "Optical chemosensors for the gas phase detection of aldehydes: mechanism, material design, and application," Mater. Adv. **2**(19), 6213–6245 (2021).

30. Y. Yu, X. Gai, P. Ma, K. Vu, Z. Yang, R. Wang, D.-Y. Choi, S. Madden, and B. Luther-Davies, "Experimental demonstration of linearly polarized 2-10 μm supercontinuum generation in a chalcogenide rib waveguide," Opt. Lett. **41**(5), 958–961 (2016).

31. D.-Y. Choi, S. Madden, A. Rode, R. Wang, and B. Luther-Davies, "Fabrication Process Development for As$_2$S$_3$ Planar Waveguides using Standard Semiconductor Processing," in *COIN-ACOFT 2007 - Joint International Conference on the Optical Internet and the 32nd Australian Conference on Optical Fibre Technology*, (2007), pp. 1–3.

32. J. Chiles, M. Malinowski, A. Rao, S. Novak, K. Richardson, and S. Fathpour, "Low-loss, submicron chalcogenide integrated photonics with chlorine plasma etching," Appl. Phys. Lett. **106**(11), 111110 (2015).

33. G. Franz, W. Hösler, and R. Treichler, "Sidewall passivation of GaAs in BCl$_3$-containing atmospheres," J. Vac. Sci. Technol. B **19**(2), 415–419 (2001).

34. A. Kobelev, N. Andrianov, A. Smirnov, and Y. Barsukov, "Boron Trichloride Dry Etching," (2016).

35. E. Sungauer, E. Pargon, X. Mellhaoui, R. Ramos, G. Cunge, L. Vallier, O. Joubert, and T. Lill, "Etching mechanisms of HfO$_2$, SiO$_2$, and poly-Si substrates in BCl$_3$ plasmas," J. Vac. Sci. Technol. B **25**(5), 1640–1646 (2007).

36. J. H. Muessig, P. Lisinetskaya, R. D. Dewhurst, R. Bertermann, M. Thaler, R. Mitric, and H. Braunschweig, "Tetraiododiborane(4) (B$_2$I$_4$) is a Polymer Based on sp$^3$ Boron in the Solid State," Angew. Chem. Int. Ed. **59**(14), 5531–5535 (2020).

37. A. M. Morrison, T. Liang, and G. E. Douberly, "Automation of an "Aculight" continuous-wave optical parametric oscillator," Rev. Sci. Instrum. **84**(1), 013102 (2013).

38. Z. Yang, R. Zhang, Z. Wang, P. Xu, W. Zhang, Z. Kang, J. Zheng, S. Dai, R. Wang, and A. Majumdar, "High-Q, submicron-confined chalcogenide microring resonators," Opt. Express **29**(21), 33225–33233 (2021).

39. M. Grayson, "Chalcogenide Photonic Devices for the Near to Far Infrared," PhD Thesis, University of Colorado Boulder (2022).

40. H. Lin, Y. Xiang, L. Li, K. McLaughlin, Y. Liu, Y. Chillakuru, E. Koontz, J. D. Musgraves, K. Richardson, C. Ni, and J. Hu, "High-Q Mid-Infrared Chalcogenide Glass Resonators for Chemical Sensing," in *2014 IEEE Photonics Society Summer Topical Meeting Series*, (2014), pp. 61–62.

41. Z. Tang, V. S. Shiryaev, D. Furniss, L. Sojka, S. Sujecki, T. M. Benson, A. B. Seddon, and M. F. Churbanov, "Low loss ge-as-se chalcogenide glass fiber, fabricated using extruded preform, for mid-infrared photonics," Opt. Mater. Express **5**(8), 1722–1737 (2015).

42. H. Parnell, D. Furniss, Z. Tang, Y. Fang, T. M. Benson, C. L. Canedy, C. S. Kim, M. Kim, C. D. Merritt, W. W. Bewley, I. Vurgaftman, J. R. Meyer, and A. B. Seddon, "High purity ge-sb-se/s step index optical fibers," Opt. Mater. Express **9**(9), 3616–3626 (2019).

43. O. Kondrat, N. Popovich, R. Holomb, V. Mitsa, V. Lyamayev, N. Tsud, V. Cháb, V. Matolín, and K. C. Prince, "Synchrotron radiation photoelectron spectroscopy studies of self-organization in As$_{40}$Se$_{60}$ nanolayers stored under ambient conditions and after laser irradiation," J. Non-Cryst. Solids **358**(21), 2910–2916 (2012).

44. J. Hu, N. Carlie, L. Petit, A. Agarwal, K. Richardson, and L. C. Kimerling, "Cavity-Enhanced IR Absorption in Planar Chalcogenide Glass Microdisk Resonators: Experiment and Analysis," J. Lightwave Technol. **27**(23), 5240–5245 (2009).

45. A. Gutierrez-Arroyo, E. Baudet, L. Bodiou, J. Lemaitre, I. Hardy, F. Faijan, B. Bureau, V. Nazabal, and J. Charrier, "Optical characterization at 7.7 μm of an integrated platform based on chalcogenide waveguides for sensing applications in the mid-infrared," Opt. Express **24**(20), 23109–23117 (2016).

46. M. Baillieul, E. Baudet, K. Michel, J. Moreau, P. Nemec, K. Boukerma, F. Colas, J. Charrier, B. Bureau, E. Rinnert, and V. Nazabal, "Toward Chalcogenide Platform Infrared Sensor Dedicated to the In Situ Detection of Aromatic Hydrocarbons in Natural Waters via an Attenuated Total Reflection Spectroscopy Study," Sensors **21**(7), 2449 (2021).

47. C. Charlton, A. Katzir, and B. Mizaikoff, "Infrared Evanescent Field Sensing with Quantum Cascade Lasers and Planar Silver Halide Waveguides," Anal. Chem. **77**(14), 4398–4403 (2005).

48. B. Schwarz, P. Reininger, D. Ristanic, H. Detz, A. M. Andrews, W. Schrenk, and G. Strasser, "Monolithically integrated mid-infrared lab-on-a-chip using plasmonics and quantum cascade structures," Nat. Commun. **5**(1), 4085 (2014).

49. A. Nitkowski, L. Chen, and M. Lipson, "Cavity-enhanced on-chip absorption spectroscopy using microring resonators," Opt. Express **16**(16), 11930–11936 (2008).